

# Multipath Doppler Difference Estimation in Over-the-Horizon Radar

Yimin D. Zhang<sup>†</sup> and Braham Himed<sup>‡</sup>

<sup>†</sup> Department of Electrical and Computer Engineering

Temple University, Philadelphia, PA 19122, USA

<sup>‡</sup> RF Technology Branch, Air Force Research Laboratory

AFRL/RVMD, Dayton, OH 45433, USA

**Abstract**—Target altitude estimation is an important and challenging task in over-the-horizon radar. It has been shown that the elevation motion of a maneuvering target can be effectively revealed by local multipath signals which generally contain three distinct components with highly time-varying and closely separated Doppler signatures. Because of the close separation between the Doppler signatures, it is challenging to accurately estimate the Doppler frequency difference. In this paper, we develop a low-complexity technique that effectively estimates the Doppler frequency difference by utilizing the a priori knowledge of the Doppler characteristics of the local multipath signals. The effectiveness of the proposed method is verified using simulated results.

**Keywords**—Doppler signature, over-the-horizon radar, target geolocation, time-frequency analysis.

## I. INTRODUCTION

By utilizing ionospheric reflections, skywave over-the-horizon radar (OTHR) systems are designed to perform target detection over a wide surveillance area that is significantly beyond the limit of the Earth horizon. OTHRs are typically operated in the high frequency (HF) band with a narrow signal bandwidth that is determined based on the ionospheric conditions and the target range [1]. Limited by the signal bandwidth and the instability of the ionosphere layers, the range resolution of an OTHR system is typically in the order of kilometers or tens of kilometers [2].

An important task in OTHR operations is to determine the geolocation of the targets, particularly the target altitude information [3–5]. In particular, the target altitude information is valuable in determining the class of the targets. Nevertheless, direct estimation of target altitude is generally infeasible because of the poor range resolution associated with the very narrow bandwidth of the OTHR waveforms. In practice, the ground or ocean reflections nearby the targets generates so-called local multipath signals which can be used to reveal the elevation motion of the targets [6]. More specifically, signals directly reflected by the ionosphere layers and those also reflected by ground/ocean surface would generate slightly

different Doppler signatures when a target maneuvers vertically. That is, different multipath signals manifest themselves as different non-linear time-frequency trajectories, each corresponding to a Doppler signature of the target along a different round-trip propagation path [3, 5]. It has been shown in [3, 5] that high-resolution time-frequency analysis of the Doppler signatures can resolve Doppler signatures, enabling fast and robust altitude tracking. Nevertheless, due to the close separation between the Doppler signatures and their non-linearity, accurate estimation of the Doppler frequency difference is often complicated and even difficult. Existing techniques require extensive parametric analysis with a high complexity [5, 7, 8].

In this paper, we develop a low-complexity technique for the estimation of the Doppler frequency difference. By taking advantages of the *a priori* knowledge that, in the underlying application, the multipath signals comprise three components with close and symmetric frequency characteristics, the proposed technique is based on simple multiplication of the received multi-component signal waveform with its complex conjugate. As a result, the squared magnitude operation precisely removes the nominal components and generates four symmetric components, which are associated as positive and negative harmonics, and a direct current (DC) component. Therefore, the estimation of target Doppler frequency can be solved using conventional time-frequency analysis, such as short-time Fourier transform. The effectiveness of the proposed method is verified using simulated results.

## II. SIGNAL MODEL

### A. Multipath Propagation Geometry

Consider a flat-earth ionosphere model as shown in Fig. 1, where  $H$  is the height of the ionosphere layer, and  $h$  is the height of the target [5]. We only consider propagation through the stable E-layer of ionosphere and its height,  $H$ , is considered constant over the processing time and is known (an OTHR system periodically monitors the ionosphere conditions). In this figure, the targets and propagation paths below the ionosphere are the true ones, whereas those above the ionosphere illustrate their images through the ionosphere layer and ground reflections for the convenience of slant range computations.

---

The work of Y. D. Zhang is supported in part by a subcontract with Matrix Research, Inc. for research sponsored by the Air Force Research Laboratory under contract FA8650-14-D-1722.

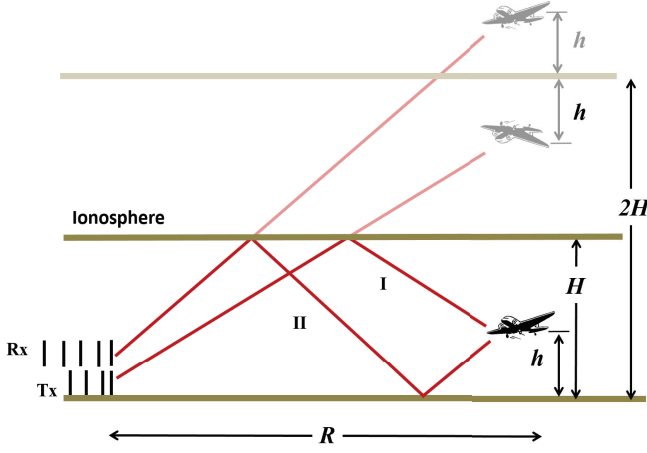


Fig. 1. Flat-earth model of local multipath propagation in an OTHR system.

As we observe in Fig. 1, the local multipath around a target, due to earth surface reflections, yields different propagation paths of the emitted/received signals which are represented by the following three groups of signals. For the first component, both the emitted and received signals propagate along path I, whereas for the second component, both the emitted and received signals propagate along path II. The third component comprises two paths, one emitting along path I and returning back along path II, and the other emitting along path II and returning back along path I.

From Fig. 1, the slant ranges  $l_1$  and  $l_2$  can be expressed in terms of the ground range  $R$ , the ionosphere altitude  $H$ , and the target altitude  $h$ , as

$$l_1 = (R^2 + (2H - h)^2)^{1/2}, \quad l_2 = (R^2 + (2H + h)^2)^{1/2}. \quad (1)$$

In practice,  $R \gg H \gg h$  holds, and the relationship between the slant ranges and the other parameters can be better revealed by the following approximations:

$$l_1 \approx R + \frac{2H^2 - 2Hh}{R}, \quad l_2 \approx R + \frac{2H^2 + 2Hh}{R}. \quad (2)$$

### B. Doppler Characteristics

For a maneuvering target, its horizontal and elevation motions generate different Doppler frequency characteristics. To analyze such effects, we denote the target horizontal velocity as  $\dot{R}(t) = dR(t)/dt$ , and vertical velocity as  $\dot{h}(t) = dh(t)/dt$ . Note here that we have introduced  $t$  in the range and the target altitude to emphasize their time dependency. From (2), we obtain

$$\begin{aligned} \frac{dl_1(t)}{dt} &\approx K(t)\dot{R}(t) - \frac{2H}{R(t)}\dot{h}(t), \\ \frac{dl_2(t)}{dt} &\approx K(t)\dot{R}(t) + \frac{2H}{R(t)}\dot{h}(t), \end{aligned} \quad (3)$$

where  $K(t) = 1 - 2H^2/R^2(t)$ . The Doppler frequencies of

the three different paths are then respectively obtained as

$$\begin{aligned} f_{D,1}(t) &= -\frac{2f_c}{c} \frac{dl_1(t)}{dt} \approx -\frac{2f_c}{c} K(t)\dot{R}(t) + \frac{4f_c H}{R(t)c} \dot{h}(t), \\ f_{D,2}(t) &= -\frac{2f_c}{c} \frac{dl_2(t)}{dt} \approx -\frac{2f_c}{c} K(t)\dot{R}(t) - \frac{4f_c H}{R(t)c} \dot{h}(t), \\ f_{D,3}(t) &= -\frac{f_c}{c} \frac{dl_1(t) + dl_2(t)}{dt} \approx -\frac{2f_c}{c} K(t)\dot{R}(t), \end{aligned} \quad (4)$$

where  $f_c$  is the carrier frequency, and  $c$  is the velocity of the electromagnetic wave.

By further denoting  $\bar{f}_D(t) = -2f_c K(t)\dot{R}(t)/c$  as the nominal Doppler component, and  $\tilde{f}_D(t) = 4f_c H \dot{h}(t)/[R(t)c]$  as the differential component, then the above expressions can be reformulated as

$$\begin{aligned} f_{D,1}(t) &= \bar{f}_D(t) + \tilde{f}_D(t), \\ f_{D,2}(t) &= \bar{f}_D(t) - \tilde{f}_D(t), \\ f_{D,3}(t) &= \bar{f}_D(t). \end{aligned} \quad (5)$$

Therefore, the Doppler signatures for the first path and the second path are symmetric around that of the third path. The nominal Doppler component,  $\bar{f}_D(t)$ , is shared by all the three paths and reveals the target velocity in the range direction, whereas the small Doppler difference between the paths,  $\tilde{f}_D(t)$ , is a function of  $\dot{h}(t)$  and thus reveals the vertical maneuvering of the target [5, 7, 8]. As such, it becomes important to estimate  $\tilde{f}_D(t)$  for the purpose of target altitude estimation and tracking. However, as  $\tilde{f}_D(t)$  is very small as compared to the variations of  $\bar{f}_D(t)$ , it is often difficult to resolve the three components, making the estimation of  $\tilde{f}_D(t)$  challenging.

## III. ESTIMATION OF DOPPLER DIFFERENCE

### A. Removal of Nominal Doppler Component

Under this assumption, the received signal can be expressed as:

$$x(t) = A_1 \exp(j\phi_1(t)) + A_2 \exp(j\phi_2(t)) + A_3 \exp(j\phi_3(t)), \quad (6)$$

where  $A_i$  and  $\phi_i(t)$  are, respectively, the path loss and the instantaneous phase law of the  $i$ th path for  $i = 1, 2$ , and 3.

The phase laws can be expressed as

$$\phi_i(t) = -2\pi \int_0^t f_{D,i}(t) dt = \frac{4\pi f_c}{c} \left[ K(t)R(t) - \frac{2\xi_i H}{R(t)} h(t) \right], \quad (7)$$

where  $\xi_1 = -1$ ,  $\xi_2 = 1$ , and  $\xi_3 = 0$ . Note that the local multipath based approach does not reveal the sign of the Doppler frequency difference because of the symmetry in (6).

For clarity, we denote  $\theta(t) = (4\pi f_c/c)K(t)R(t)$  and  $\psi(t) = -(4\pi f_c/c)(2\xi_i H h(t)/R(t))$ . Then, (7) can be written as

$$\phi_1(t) = \theta(t) - \psi(t), \quad \phi_2(t) = \theta(t) + \psi(t), \quad \phi_3(t) = \theta(t). \quad (8)$$

For the purpose of estimating the target manoeuvring velocity in the elevation dimension, we only need to estimate  $\psi(t)$  from

the received signal. Toward this end, we multiply  $x(t)$  with its conjugation,  $x^*(t)$ , and obtain

$$\begin{aligned} |x(t)|^2 &= x(t)x^*(t) \\ &= (|A_1|^2 + |A_2|^2 + |A_3|^2) \\ &\quad + (A_1A_3^* + A_2^*A_3) \exp(-j\psi(t)) \\ &\quad + (A_1^*A_3 + A_2A_3^*) \exp(j\psi(t)) \\ &\quad + A_1A_2^* \exp(-j2\psi(t)) + A_1^*A_2 \exp(j2\psi(t)). \end{aligned} \quad (9)$$

It is clear from the above expression that the resulting product  $|x(t)|^2$  no longer contains  $\theta(t)$ . Rather, it contains a DC component, the phase difference term  $\exp(j\psi(t))$ , its second-order harmonic, and the image of the last two terms at the negative frequencies. The four frequency components are demodulated and localized in the close vicinity of the DC frequency, and thus can be clearly resolved in the time-frequency domain through spectral analysis with the use of a long window.

The concept of demodulating Doppler signatures associated with local multipath signals in OTHR was first discussed in [8] and was later elaborated in [5] where the nominal Doppler frequency is estimated using time-frequency analysis techniques. It generally yields inaccurate nominal Doppler frequency estimation and the processing is highly time-consuming. Compared with such existing methods, the proposed method does not require such Doppler estimation procedure, yielding much simpler and more accurate Doppler signature demodulations.

In the following, we describe a simple technique to visualize the time-frequency characteristics of the Doppler frequency difference and estimate the instantaneous frequency difference signature using the conventional short-time Fourier transform (STFT) method [9, 10]. Other methods, including sparse reconstruction methods recently developed for time-frequency analysis [11–15], can also be used for the visualization and analysis of the Doppler frequency differences.

### B. Time-Frequency Analysis and Doppler Detection

The STFT of the squared magnitude of the signal,  $|x(t)|^2$ , is expressed as

$$X(t, f) = \int_{-\infty}^{\infty} |x(u)|^2 g(t-u) \exp(-j2\pi fu) du, \quad (10)$$

where  $g(t)$  is a window function. Note that  $X(t, f)$  contains four harmonic components with non-zero frequencies. To further enhance the Doppler signature and avoid the estimation ambiguity between the harmonic components, we can fuse the information contained in the four non-zero frequency signatures by computing the following quantity:

$$Y(t, f) = X(t, f)X\left(t, \frac{f}{2}\right) + X(t, -f)X\left(t, -\frac{f}{2}\right). \quad (11)$$

Note that  $Y(t, f)$  is symmetric in frequency about the DC, so we only need to analyze the positive frequency side. The Doppler frequency at each time instant can be detected through peak value detection.

TABLE I. KEY PARAMETERS

Parameter	Notation	Value
initial range	$R(0)$	1,500 km
ionosphere height	$H$	160 km
aircraft initial height	$h(0)$	10,000 m
horizontal target velocity	$v_{R,\max}$	175 m/s
maximum descending velocity	$v_{c,\max}$	19.68 m/s
carrier frequency	$f_c$	16 MHz
waveform repetition frequency	$f_s$	40 Hz

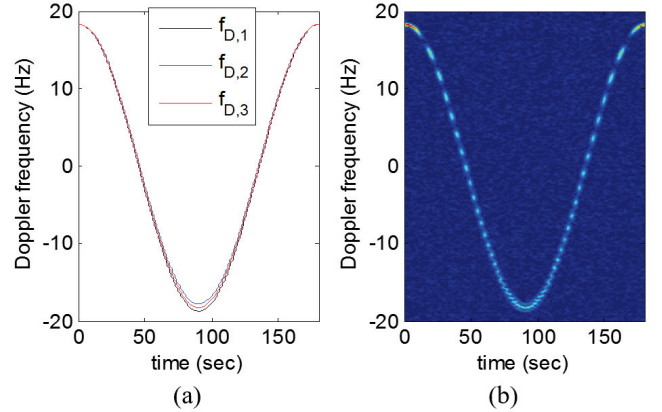


Fig. 2. Doppler signature and spectrogram of  $x(t)$ . (a) True Doppler signature. (b) Spectrogram.

## IV. SIMULATION RESULTS

### A. Operation Scenario

In this section, simulation results are presented to verify the effectiveness of the proposed technique and examine the performance with different parameters. As an example, we consider a maneuvering aircraft which makes a  $360^\circ$  circular turn of radius 5 km in approximately  $T = 179.5$  seconds to descend by approximately 2,250 meters [5]. The center of the transmit and receive arrays is set as the coordinate origin. The other key parameters used in the simulations are listed in Table I. All the multipath signals are considered to fall within the same range cell. The aircraft maintains an horizontal velocity of 175 m/s (630 km/hr). Its elevation velocity varies sinusoidally and the corresponding target altitude is expressed as

$$h(t) = h(0) - \frac{v_{c,\max}T_0}{\pi} \left[ 1 - \cos\left(\frac{\pi t}{T_0}\right) \right], \quad (12)$$

and the corresponding elevation velocity is obtained as

$$\tilde{f}_D = \frac{4f_c H}{R(t)c} \dot{h}(t) = -\frac{4f_c H v_{c,\max} T_0}{R(t)c} \sin\left(\frac{\pi t}{T_0}\right). \quad (13)$$

As such, the Doppler frequency difference  $\tilde{f}_D(t)$  is sinusoidal and, for the parameters given in Table I, the peak Doppler frequency difference is 0.4478 Hz. The maximum frequency of the nominal Doppler frequency component,  $\tilde{f}_D(t)$ , is 18.66 Hz.

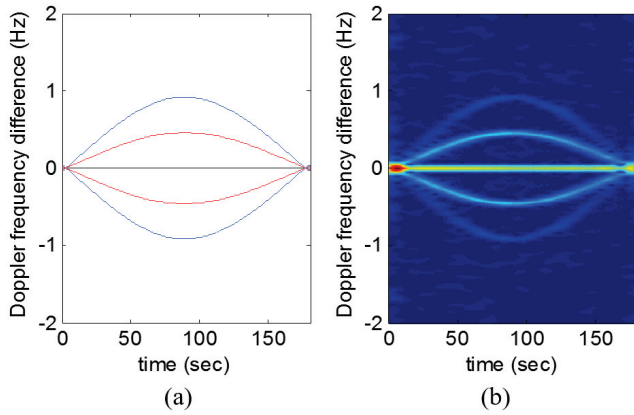


Fig. 3. Doppler signature and spectrogram of the squared magnitude of the signal,  $|x(t)|^2$ . (a) True signature of the Doppler frequency difference. (b) Spectrogram.

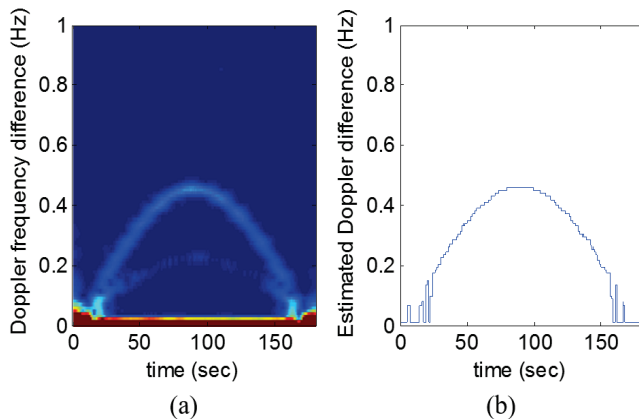


Fig. 4. Spectrogram of  $Y(t, f)$  and the Doppler difference signature estimated through peak detection. (a) Spectrogram. (b) Estimated Doppler difference signature.

### B. Processed Results

The actual Doppler signatures of the three-component multipath signal obtained from (6) are depicted in Fig. 2(a). The clutter is ignored for presentation succinctness. In practice, the clutter can be filtered out using, e.g., the autoregressive (AR) pre-whitening techniques [3, 16]. The corresponding spectrogram, which is defined as the squared magnitude of  $X(t, f)$ , is shown in Fig. 2(b). The input signal-to-noise ratio (SNR) is set to 0 dB. In practice, this input SNR is evaluated after receive array beamforming or multiple-input multiple-output (MIMO) radar combining. Because of the very close frequency separation on the highly dynamic nominal Doppler signatures, separation of these Doppler signatures for the individual Doppler frequency has been shown to be challenging unless an estimation of these signatures is made and the signals are made stationary [5, 8].

Figs. 3(a) and 3(b) show the true Doppler signature of  $|x(t)|^2$  and the corresponding spectrogram. It is clear that

the Doppler frequency difference is clearly revealed through standard STFT operations. To further enhance the result, we perform the operation depicted in (11), and the result of  $Y(t, f)$  is shown in Fig. 4(a). Due to symmetry, only the positive frequency portion is shown. Fig. 4(b) shows the estimated Doppler difference through peak detection of  $|Y(t, f)|^2$ . Except for the edge portion in which the multipath components with close frequencies interfere, the estimated Doppler difference generally well coincides with the true Doppler difference as depicted by the red lines in Fig. 3(a).

## V. CONCLUSION

We have developed a novel method that reveals the Doppler difference between multipath signals in over-the-horizon operation. This significantly simplifies the Doppler difference estimation, facilitating real-time analysis of target altitudes. We have verified the effectiveness of the proposed method using simulated data that closely model real target manoeuvrability. Compared with existing methods, the proposed technique is much simpler and more robust.

## REFERENCES

- [1] J. M. Headrick and S. J. Anderson, "HF over-the-horizon radar," Chapter 20 in M. Skolnik (ed.), *Radar Handbook, 3rd Ed.* McGraw-Hill, 2008.
- [2] G. A. Fabrizio (ed.), *High Frequency Over-the-Horizon Radar: Fundamental Principles, Signal Processing, and Practical Applications.* McGraw-Hill, 2013.
- [3] Y. Zhang, M. G. Amin, and G. J. Frazer, "High-resolution timefrequency distributions for manoeuvring target detection in over-the-horizon radars," *IEE Proc.-Radar Sonar Navig.*, vol. 150, no. 4, pp. 299–304, 2003.
- [4] Y. D. Zhang, M. G. Amin, and B. Himed, "Altitude estimation of maneuvering targets in MIMO over-the-horizon radar," in *Proc. IEEE Sensor Array and Multichannel Signal Process. Workshop*, Hoboken, NJ, 2012, pp. 257–260.
- [5] Y. D. Zhang, J. J. Zhang, M. G. Amin, and B. Himed, "Instantaneous altitude estimation of maneuvering targets in over-the-horizon radar exploiting multipath Doppler signatures," *EURASIP J. Adv. Signal Process.*, vol. 2013, no. 2013:100, pp. 1–13, May 2013.
- [6] R. H. Anderson, S. Kraut, and J. L. Krolik, "Robust altitude estimation for over-the-horizon radar using a state-space multipath fading model," *IEEE Trans. Aerospace Electron. Syst.*, vol. 39, no. 1, pp. 192–201, 2003.
- [7] C. Ioana, M. G. Amin, Y. D. Zhang, and F. Ahmad, "Characterization of Doppler effects in the context of over-the-horizon radar," in *Proc. IEEE Radar Conf.*, Washington, D.C., 2010, pp. 506–510.
- [8] C. Ioana, Y. D. Zhang, M. G. Amin, F. Ahmad, G. Frazer, and B. Himed, "Time-frequency characterization of micro-multipath signals in over-the-horizon radar," in *Proc. IEEE Radar Conf.*, Atlanta, GA, 2012, pp. 671–675.
- [9] L. Cohen, *Time-Frequency Analysis.* Prentical Hall, 1995.
- [10] V. Chen and H. Ling, *Time-Frequency Transforms for Radar Imaging and Signal Analysis.* Aetech House, 2002.

- [11] P. Flandrin and P. Borgnat, "Time-frequency energy distributions meet compressed sensing," *IEEE Trans. Signal Process.*, vol. 58, no. 6, pp. 2974–2982, June 2010.
- [12] Y. D. Zhang, M. G. Amin, and B. Himed, "Reduced interference time-frequency representations and sparse reconstruction of undersampled data," in *Proc. European Signal Process. Conf.*, Marrakech, Morocco, Sept. 2013, pp. 1–5.
- [13] B. Boashash (ed.), *Time-Frequency Signal Analysis and Processing, 2nd Ed.* Academic Press, 2015.
- [14] Y. D. Zhang and B. Wang, "Group sparsity based estimation of harmonic speech signals," in *Proc. SPIE Compressive Sensing Conf.*, vol. 9484, Baltimore, MD, April 2015.
- [15] M. G. Amin, B. Jakonovic, Y. D. Zhang, and F. Ahmad, "A sparsity-perspective to quadratic time-frequency distributions," *Digital Signal Process.*, vol. 46, pp. 175–190, Nov. 2015.
- [16] T. J. Nohara and S. Haykin, "AR-based growler detection in sea clutter," *IEEE Trans. Signal Process.*, vol. 41, no. 3, pp. 1259–1271, March 1993.